

## An unusual occurrence of coesite at the Lonar crater, India

Steven J. JARET<sup>1\*</sup>, Brian L. PHILLIPS<sup>1</sup>, David T. KING JR<sup>2</sup>, Tim D. GLOTCH<sup>1</sup>, Zia RAHMAN<sup>3</sup>,  
and Shawn P. WRIGHT<sup>4</sup>

<sup>1</sup>Department of Geosciences, Stony Brook University, Stony Brook, New York 11794–2100, USA

<sup>2</sup>Department of Geosciences, Auburn University, Auburn, Alabama 36849, USA

<sup>3</sup>Jacobs—NASA Johnson Space Center, Houston, Texas 77058, USA

<sup>4</sup>Planetary Science Institute, Tucson, Arizona 85719, USA

\*Corresponding author. E-mail: steven.jaret@stonybrook.edu

(Received 18 March 2016; revision accepted 06 September 2016)

---

**Abstract**—Coesite has been identified within ejected blocks of shocked basalt at Lonar crater, India. This is the first report of coesite from the Lonar crater. Coesite occurs within SiO<sub>2</sub> glass as distinct ~30 μm spherical aggregates of “granular coesite” identifiable both with optical petrography and with micro-Raman spectroscopy. The coesite+glass occurs only within former silica amygdules, which is also the first report of high-pressure polymorphs forming from a shocked secondary mineral. Detailed petrography and NMR spectroscopy suggest that the coesite crystallized directly from a localized SiO<sub>2</sub> melt, as the result of complex interactions between the shock wave and these vesicle fillings.

---

### INTRODUCTION

#### High-Pressure SiO<sub>2</sub> Phases

Silica (SiO<sub>2</sub>) polymorphs are some of the simplest minerals in terms of elemental chemistry, yet they are structurally complex with over 30 stable or metastable phases (Heaney et al. 1994). Two important polymorphs found in impactites are the high-pressure, high-temperature polymorphs coesite and stishovite. The first of these, coesite, is thermodynamically stable above 500 °C and 2.5 GPa (Liu and Bassett 1986; Zhang et al. 1996; Fei and Bertka 1999). Crystallographically, coesite has monoclinic symmetry, but typically forms pseudo-hexagonal flakes when produced experimentally (Coes 1953; Ramsdell 1955). Coesite can be distinguished from quartz optically as it has a refractive index of 1.59–1.604 and a density of 3.0 g cm<sup>-3</sup>, compared to values of 1.54–1.55 and 2.65 for quartz.

The second high-pressure silica polymorph, stishovite (Stishov and Papova 1961; Chao et al. 1962; Stöffler 1971) forms at higher pressure-temperature conditions than coesite. Natural stishovite has only been reported from meteorites and terrestrial impactites (Ferrière and Osinski 2013), where it is thought to form as a direct response to shock loading (Stöffler 1971).

Although there is no direct observation of nonshock stishovite in nature, a possible post-stishovite phase may be a large component of subducting slabs and the core-mantle boundary (Lakshtanov et al. 2007), and stishovite likely occurs in the deep mantle if basaltic slabs survive to depth. Additionally, two SiO<sub>2</sub> phases denser than stishovite have been identified in Martian shergottites (El Goresy et al. 2001b, 2008).

Coesite was first produced experimentally (Coes 1953; Ramsdell 1955) and was subsequently identified in natural materials from the Meteor Crater, Arizona (Chao et al. 1960). Since then, coesite has been widely known as a shock feature related to impact events, although it also occurs in nonimpact rocks such as kimberlites (Smyth and Hatton 1977), and as inclusions within ultrahigh-pressure eclogites (Chopin 1984; Smith 1984). Because of these nonimpact occurrences, coesite can only be diagnostic of impact events if found in shallow crustal or surficial rocks and/or in a geologic context that sufficiently rules out high-pressure metamorphic conditions (French and Koeberl 2010).

Despite often being described as an impact product, coesite has not been widely reported at terrestrial impact sites, having been identified at only 30 of the 186 (17%) known craters to date (Fig. 1; Table 1). Furthermore, descriptions and interpretations of

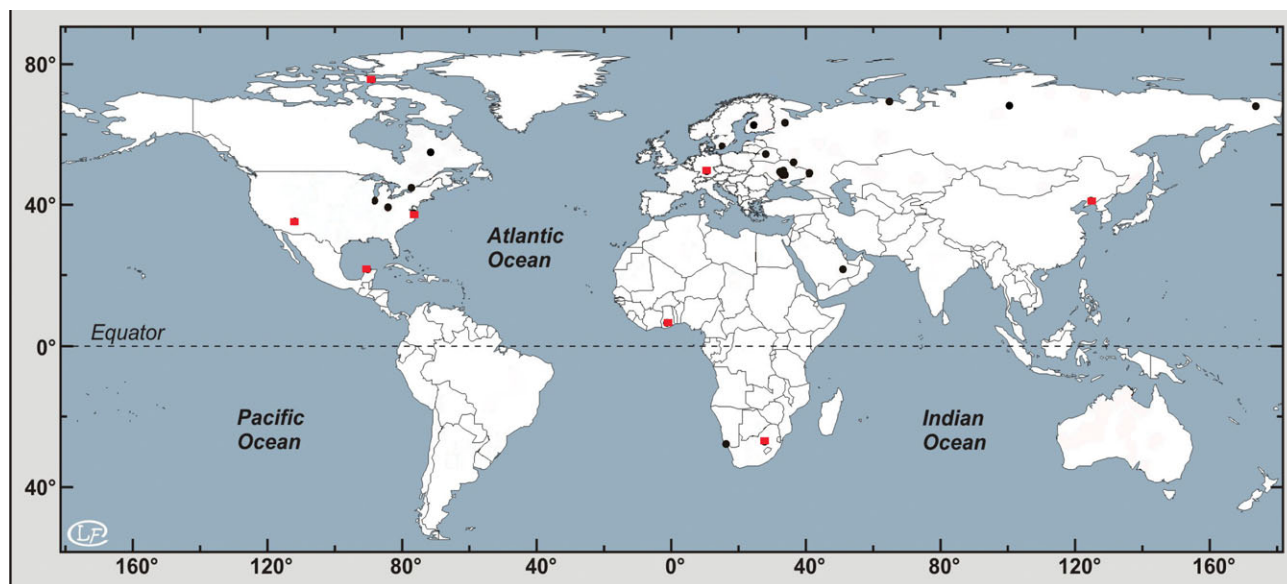


Fig. 1. Structures with reports of coesite. Structures with reports of coesite that include petrographic context are shown in red boxes. All are modified after L. Ferrière (<http://www.meteorimpactonearth.com/meteorite.html>). References used are listed in Table 1.

formation conditions regarding impact-produced coesite are commonly lacking. Of the 30 reports of coesite at impact structures, only 8 (4%) of those provide detailed petrographic context of the coesite (Table 1).

### Coesite Formation Conditions

Many details of the quartz-coesite transformation remain unclear. Particularly in the impact setting, two remaining questions are (1) the role of melting and (2) whether or not coesite can crystallize out of a melt or if it forms as a solid-state transformation. In impact settings, coesite is most commonly interpreted to have formed via solid-state phase transformations that are associated with diaplectic quartz (Stöffler 1971; Kieffer et al. 1976; Stähle et al. 2008; Ferrière and Osinski 2013).

In some instances, impact-generated coesite is interpreted to have formed at high pressure after stishovite or a stishovite-like metastable phase (Stöffler 1971; Kleeman and Ahrens 1973). This hypothesis is based on observations made on samples taken at Ries crater, where stishovite and coesite co-occur but the coesite cuts across lamellar structures, which contain stishovite. In this instance, coesite is thought to form behind the shock front, via pressure release from a stishovite-like phase (Dachille et al. 1963), or after pressure release from a silica phase of short-range order with four-fold coordination of Si (Stöffler 1971).

Formation on pressure release may not be the only way coesite can develop. For example, coesite in

terrestrial ultrahigh-pressure samples (i.e., eclogites) is thought to form on compression, as supported by in situ analyses of experiments at high pressure, which capture the quartz-coesite transition before the sample is released from high pressure (Perrillat et al. 2003). When coesite forms on compression, the higher pressure phase stishovite is not required. Additionally, the quartz-coesite transformation conditions can vary depending on porosity and water content of the rock. In nonporous rocks, coesite formation requires pressures of 12–45 GPa, whereas porous rocks may only require 7–8 GPa (Osinski 2007). It is worth noting, however, that comparisons between static (e.g., eclogites) and dynamic (impact) coesite formation may be complicated because of sluggish kinetics of the reconstructive transition.

Because of the common association of impact-produced coesite with diaplectic quartz, the formation of coesite in this setting may require slightly longer shock pulses. Formation of coesite in association with diaplectic quartz may be restricted to >30 GPa, which is over 10 times greater than the pressure required in static equilibrium coesite synthesis (De Carli and Milton 1965; Stöffler 1971).

Furthermore, it remains uncertain if coesite forms only by solid-state processes or if it can also form as a direct crystallization product of silica-rich melts at high pressure. Synthetic coesite has only been produced in the lab via solid-state experiments, and impact-produced coesite is most commonly interpreted as a solid-state transition. However, Chen et al. (2010), suggested that

Table 1. Reports of natural impact related coesite.

Structure	Country	Authors	Description	Method of identification
Bolysh	Ukraine	Gurov et al. (1980)	None given	HF dissolution; X-ray identification
Bosumtwi	Ghana	Littler (1962)	In non vesicular glass (presumably lechatelierite)	HF dissolution; X-ray diffraction
Bosumtwi	Ghana	Morrow (2007)	Rare, but associated with diaplectic quartz; highly refractive, light green grains and beaded aggregates less than 50 $\mu\text{m}$	Micro-Raman spectroscopy
Bosumtwi	Ghana	Ferrière et al. (2009)	Light green, highly refractive inclusions (<3 $\mu\text{m}$ ) in ballen type I and as green 30- $\mu\text{m}$ aggregates	Micro-Raman spectroscopy
Chesapeake Bay	USA	Jackson et al. (2016)	Coesite occurs within suevitic breccias	Micro-Raman spectroscopy, X-ray diffraction, optical petrography
Chesapeake Bay	USA	Horton et al. (2009)	Occurs in suevites	Acid dissolution of whole rock splits; X-ray diffraction; micro-Raman spectroscopy
Chicxulub	Mexico	Lounejeva et al. (2002)	Up to 50 $\mu\text{m}$ brownish, well rounded polycrystalline aggregates	Micro-Raman; optical petrography
El'gygytgyn	Russia	Gurov and Koeberl (2004)	High relief veinlets in diaplectic quartz	Optical petrography; X-ray diffraction
Haughton	Canada	Osinski (2007)	High relief rims ("symplectite") around quartz grains	X-ray microdiffraction, BSE and optical petrography
Holleford	Canada	Bunch and Cohen (1963)	Refractive index of 1.593, low birefringence	Acid digestion; optical microscopy of separated grains
Ilyinets	Ukraine	Gurov et al. (1980)	None given	Enrichment by acid dissolution of quartz; X-ray identification
Jänisjärvi	Russia	Masaitis (1999)	Occurs in impact melt rocks.	None given
Kamensk	Russia	Masaitis (1999)	No description of coesite given	XRD, Raman, SEM, and electron microprobe
Kamil	Egypt	Fazio et al. (2014)	Occurs in diaplectic quartz	None given
Kara	Russia	Masaitis (1999)	Occurs as single phase and associated with glass (NOTE: does not make the distinction between diaplectic and melt glass)	None given
Kara	Russia	Vishnevskiy et al. (1977)	Occurs in brecciated rocks	X-ray diffraction, Infrared spectroscopy, optical microscopy
Kentland	USA	Cohen et al. (1961)	Associated with fused glass. Colorless to yellowish aggregates, low birefringence	HF dissolution; optical microscopy and X-ray diffraction of separates.
Lake Wanapitei	Canada	Dence et al. (1974)	Individual grains have refractive index of 1.591	HF dissolution; X-ray diffraction of mineral separates
Lappajärvi	Finland	Lehtinen (1976)	Occurs in glass-bearing samples (melt-related or solid-state glass not distinguished) Highly refractive grains	Acid digestion; X-ray diffraction and Infrared absorption spectroscopy of separates

Table 1. *Continued.* Reports of natural impact related coesite.

Structure	Country	Authors	Description	Method of identification
Logosik	Russia	Masaitis (1999)	Occurs in shocked quartz	None given
Meteor Crater	USA	Chao et al. (1960)	Texture of coesite not described other than RI	X-ray powder diffraction; optical (RI),
Mien	Sweden	Svensson and Wickman (1965)	States that coesite was identified	None given
Obolon	Russia	Gurov et al. (1980)	None given	Enrichment by acid dissolution of quartz; X-ray identification
Obolon	Russia	Masaitis (1999)	Occurs in fused glasses	None given
Popigai	Russia	Vishnevskiy et al. (2006)	Coesite has dark-blue luminescence under electronmicroprobe beam	Powder X-ray diffraction, BSE imaging
Ries	Germany	El Goresy et al. (2001a, 2001b)	Coesite occurs at grain boundaries of shocked diaplectic quartz	Micro-Raman spectroscopy, optical petrography
Ries	Germany	Stähle et al. (2008)	Granular and microcrystalline	Petrographically (optical), BSE, Laser Raman
Ries	Germany	Shoemaker and Chao (1961)	High relief, occurs in silica glass and lechatelierite	Optical microscopy; X-ray diffraction of separates
Ries	Germany	von Engelhardt and Stöffler (1968)	Fine grained aggregates in diaplectic quartz	Optical petrography (thin section)
Roter Kamm	Namibia	Hecht et al. (2008)	Thin needle-like inclusions, occurs in lechatelierite	Optical petrography (thin section)
Serpent Mound	USA	Cohen et al. (1961)	Individual grains have refractive index of 1.591	Acid digestion; optical microscopy and X-ray diffraction of separates.
Ternovka	Russia	Masaytis et al. (1980)	Brownish-yellow aggregates with refractive index of 1.593 and low birefringence. Occurs in fractures in diaplectic glass	Optical petrography (thin section); acid digestion and X-ray diffraction
Terny	Russia	Masaitis (1999)	Occurs in brecciated rocks	None given
Vredefort	South Africa	Martini (1991)	Occurs in pseudotachylites; 2 habits 1) massive coesite completely replacing quartz in the pseudotachylite. Colorless, high-relief and low-birefringent. 2) thin needles in quartz within the wall-rock	Crushed, X-ray diffraction of chips; acid digestion and X-ray diffraction of separates to concentrate coesite
Vredefort	South Africa	Martini (1978)	Occurs in pseudotachylites; granular crystals and needles up to 100 $\mu\text{m}$ long	Acid digestion; X-ray diffraction of mineral separates
Wabar	Saudi Arabia	Chao et al. (1961)	Fine grained (<5 $\mu\text{m}$ ), refractive index of 1.595, low birefringence	X-ray diffraction of bulk powders, acid digestion and optical microscopy on separates
Xiuyan	China	Chen et al. (2010)	Green aggregates of "granular coesite"	Optical petrography (thin section) and micro-Raman spectroscopy
Zapadnaya	Ukraine	Gurov et al. (2002)	Occurs in suevites and impact melt rocks	Optical microscopy

Table 1. *Continued.* Reports of natural impact related coesite.

Structure	Country	Authors	Description	Method of identification
Other natural coesite				
DSDP New Jersey		Bohor et al. (1988)	None given	X-ray diffraction
Australasian microtektite layer		Glass and Wu (1993)	None given	X-ray diffraction
North American microtektite layer		Glass and Wu (1993)	None given	X-ray diffraction
Lunar meteorite Asuka-881757		Ohtani et al. (2011)	Granular coesite. Rounded aggregates of up to 300 nm	Electron microprobe and micro-Raman spectroscopy
Eucrite meteorite, Béréba		Miyahara et al. (2014)	Granular coesite. Some are adjacent to melt veins	Raman spectroscopy and TEM

the granular coesite at the Xiuyang crater, China, crystallized from a melt. Similarly, in a review of coesite at the Ries crater, Stähle et al. (2008) interprets two petrographic types of coesite, one of which may have formed from a melt, the other likely formed in solid-state processes with either planar deformation feature (PDF) formation or diaplectic quartz.

### Identification of Coesite

Coesite can be identified optically in thin section, and nonoptically through analysis of bulk samples by techniques such as X-ray diffraction, Raman spectroscopy, infrared spectroscopy or nuclear magnetic resonance (NMR) spectroscopy. Optically, coesite is most commonly distinguished by a high refractive index (1.594) and its two morphologies: fine grained needle-like crystals (Kieffer 1971; Stöffler 1971) or as greenish aggregates (a.k.a. “granular coesite”) (Stähle et al. 2008; Chen et al. 2010). The structure of coesite is monoclinic, and the crystal system has been well defined by X-ray diffraction analysis (Levien and Prewitt 1981; Smyth et al. 1987).

### Raman Spectroscopy

Raman spectroscopy is a technique that utilizes inelastic scattering of monochromatic light to probe the vibrational modes of materials, including low-frequency crystal lattice modes. As such, this is a useful tool for distinguishing among crystal structures, especially for material of identical chemical composition such as SiO<sub>2</sub> polymorphs and glasses. Raman (and micro-Raman) spectroscopy has been used for identification of coesite in both ultrametamorphic and impact rocks (Boyer et al. 1985; El Goresy et al. 2001a; Ostroumov et al. 2002; Morrow 2007; Lu et al. 2008). Coesite exhibits a strong peak at 521  $\Delta\text{cm}^{-1}$ , which is attributed to symmetric Si-O-Si stretching mode. Additional vibrational modes include strong bands at 269 and 176  $\Delta\text{cm}^{-1}$  and slightly weaker bands at 425 and 355  $\Delta\text{cm}^{-1}$  (Sharma et al. 1983; Boyer et al. 1985; Ostroumov et al. 2002).

### Nuclear Magnetic Resonance Spectroscopy

Solid-state nuclear magnetic resonance (NMR) spectroscopy is a technique that senses nuclear spin transitions as a way of characterizing the local chemical environment (Stebbins and Xue 2014). This technique is particularly useful for analysis of amorphous material because it is sensitive only to local environment and not long-range order. Specifically for NMR, the peak position, or chemical shift, of <sup>29</sup>Si in silicates is

representative of the number and length of Si–O bonds, the types of next-nearest neighbor atoms, and other structural features such as Si–O–T bonding angles. The peak width reflects the distribution of chemical shifts, providing a measure of disorder, and the area under the peak is proportional to the number of nuclei in that local environment provided the spectra are acquired under conditions that avoid differential relaxation effects. In silicates, the <sup>29</sup>Si chemical shift is most strongly affected by coordination number. Increasing the coordination number (i.e., increasing the mean cation-oxygen distance) generally corresponds to decreasing the chemical shift (Stebbins and Xue [2014] and references therein).

Although not a routine analytical technique for impactites, NMR spectroscopy has been used previously for a few investigations of shocked quartz, coesite, and impact-produced glasses (Yang et al. 1986; Cygan et al. 1990, 1992; Boslough et al. 1993, 1995; Fiske et al. 1998; Myers et al. 1998; Lee et al. 2012).

### Lonar Crater, India

Lonar crater, India is a 1.8 km diameter crater located in Buldhana district, Maharashtra state, India (Fredriksson et al. 1973), situated within the Deccan basalt flows. This crater has been well studied (Kieffer et al. 1976; Wright et al. 2011) and is of particular interest to planetary geologists because it is the only easily accessible impact structure into only basaltic rocks, making it an attractive lunar and Martian analog (Maloof et al. 2010; Wright et al. 2011). Additionally, the composition of the Deccan basalts is similar to the surface type I spectral unit on Mars (Bandfield et al. 2000; Wright et al. 2011). The impact event is geologically recent, 570 ka (Jourdan et al. 2011), significantly younger than the 65 Ma target basalts. Importantly, during the time between the formation of the basalts and the impact event, there was significant aqueous alteration to the basalts, filling many of the basalt vesicles with zeolite, chalcedony, opal, and quartz. While these amygdules are likely hydrothermal in origin, their relationship with magmatic activity would require precise geochronology, which would be a challenge for these silica phases.

Here, we show that these secondary silica-rich phases were also shocked during the impact, producing coesite in a somewhat unusual location—only within amygdules in the vesicular basalts.

### SAMPLES

Shocked basalt, from maskelynite-bearing Class 2 through complete impact melts (aka Class 5), exists as

clasts in a ~1 m suevite breccia (aka impact melt-bearing breccia) (Kieffer et al. 1976). This unit overlies a thicker lithic breccia unit at Lonar crater (Kieffer et al. 1976; Wright et al. 2011). The three Class 2 shocked basalts (Kieffer et al. 1976) used in this study were collected in early 2010 by S. P. Wright from a suevite outcrop in the southern ejecta blanket, and were not talus. Similar to other Class 2 shocked basalts with aqueously-altered protoliths in Wright's sample collection, the three Class 2 shocked basalts examined here contain decompression cracks suggested to be due to a change in volume during compression and decompression while remaining in the solid state throughout (Wright 2013).

## METHODS

### Optical Petrography

We employed optical petrography techniques with standard-thickness, doubly polished thin sections using an Olympus BH2 petrographic microscope using 20× and 40× objectives. In a few instances, we also used some slightly thicker sections (~60 μm) when there was a concern about losing material during thin-section making. Additionally, petrography was supplemented by secondary and backscattered electron imaging using a Focused Ion Beam (FIB) system, FEI Quanta 3D FEG Dual Beam at NASA's Johnson Space Center.

The FIB cross section/slice was prepared out of the coesite+glass region using the FIB (model: FEI Quanta 3D-FEG Dual Beam, using a Ga<sup>+</sup> Ion Beam) to deposit Pt and to mill/sputter away material. The region of interest (ROI) was precisely selected and a Pt protective cap (35 μm L × 2.5 μm W × 2 μm thick) was deposited to preserve the ROI during FIB milling. After milling the front and back trenches the cross section was thinned down to ~0.5 μm and both of the faces of slice were polished using low ion beam currents in the FIB. The cross section was then undercut (U-shaped) to isolate from the bulk and when completely cut, the thin section fell inside the cavity (formed by front and back trenches). The sample was taken out from the FIB chamber and transferred to the ex situ lift-out station where a thin tip glass needle was micro manipulated to fish out the FIB prepared slice, translated and placed on a sample stub.

### Micro-Raman Spectroscopy

We collected micro-Raman spectra of polished thin sections in the Vibrational Spectroscopy Laboratory at Stony Brook University. For our measurements, we used a WiTec alpha300R confocal imaging system

equipped with 532 nm Nd YAG laser with 50 mW nominal power at the sample surface and a 50 × 0.80NA objective with a spot size of 763 nm. Raman images were acquired over a 175 × 175 μm area with acquisition times of 0.1 s. Single spectra were acquired with integration times of 60 s for coesite and 240 s for the glass.

### Magic Angle Spinning Nuclear Magnetic Resonance Spectroscopy

Silica vesicle fillings were separated from the host basalt using the Selective Fragmentation (SelFrag) electromagnetic separation instrument at Columbia University's Lamont-Doherty Earth Observatory. The separated several filling of individual vugs was crushed and ~1.5 mg of powder loaded into a 3.2 mm (OD) ZrO<sub>2</sub> rotor. The <sup>29</sup>Si MAS/NMR spectra were obtained with a 400 MHz (9.4 T) Varian Inova spectrometer operating at 79.4 MHz and a spinning rate of 12 kHz. We used 4 μs single-pulse excitation ( $\pi/2$ ) and relaxation delays ranging from 2 to 1000 s for a total of 142,000 (2 s) to 414 (1000 s) acquisitions. For some experiments, the carrier frequency and short relaxation delays (Yang et al. 1986; Myers et al. 1998) were optimized for detection of signal from stishovite, but none was observed. Clear evidence for differential relaxation was observed in the spectra, but the limited amount of sample precluded extending the relaxation delays significantly beyond 1000 s, which required nearly 5 days of acquisition time. An attempt to obtain <sup>27</sup>Al MAS/NMR data was conducted at 130.3 MHz (11.7T) and a spinning rate of 15 kHz using 1 μs pulses (4.5 μs nonselective  $\pi/2$ ) and a 2 s relaxation delay. No stishovite signal was detected.

## RESULTS

Coesite was identified in three shocked basalt samples (LC09-253, LC09-294, and LC09-256). These samples are all of shock class 2 following the classification of Kieffer et al. (1976). In these samples, plagioclase has been completely converted into solid-state maskelynite but pyroxenes retain their birefringence (as previously described by Jaret et al. 2015; Wright et al. 2011).

### Hand-Sample Petrography

In hand sample, the area of interest occurs within white amygdules (Fig. 2A). On polished slabs, two phases are recognizable based on slight differences in hue. In some instances, amygdules exhibit a milky rind in addition to bright white centers.

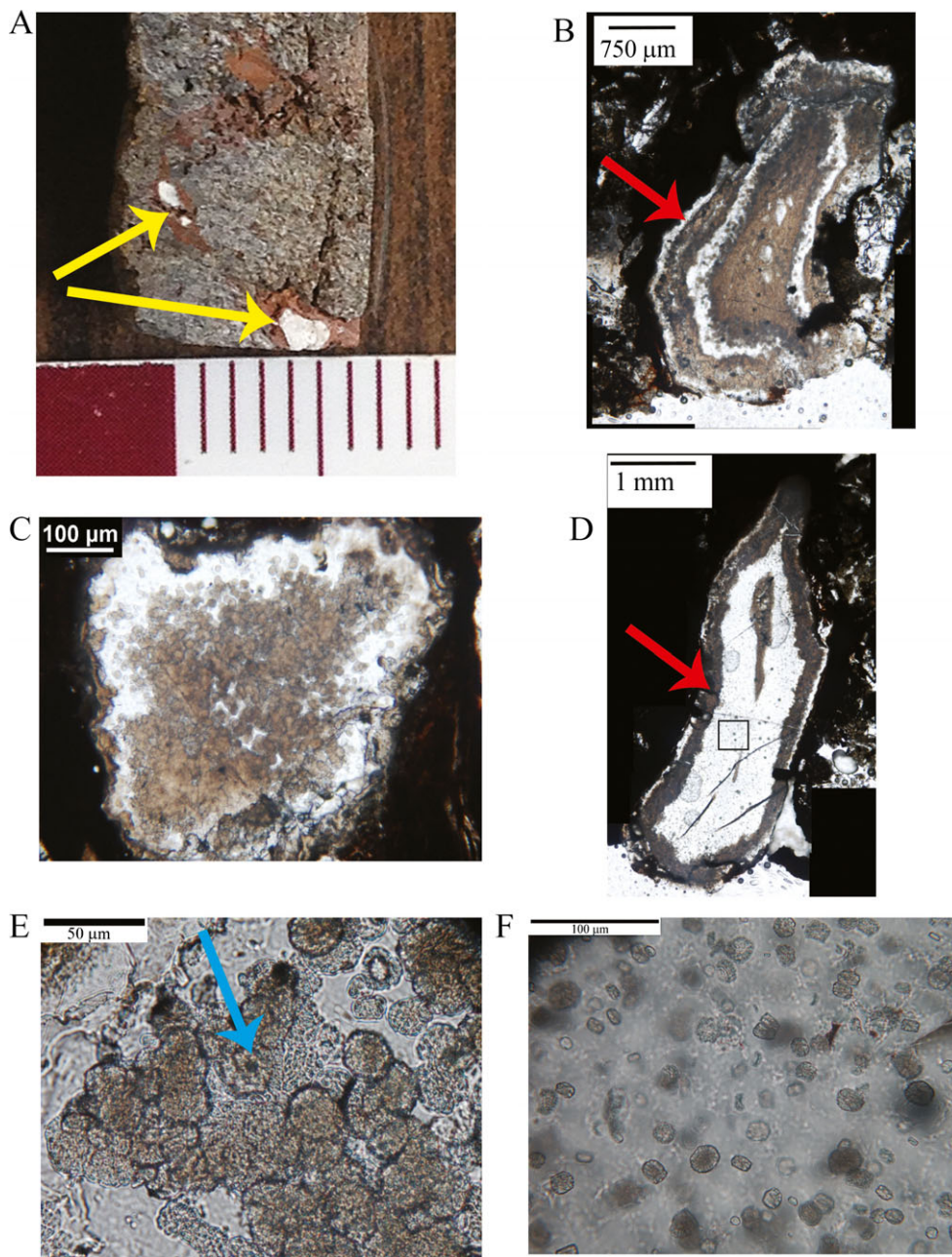


Fig. 2. Lunar coesite. A) Hand sample. Coesite occurs within the bright white amygdules (yellow arrows). Scale is in mm. B and D) plane-polarized light images (slightly thicker than standard thin-section thickness) showing granular coesite within the amygdule and as well as a rind of coesite at the edge of the amygdule (red arrow). C, E, F) Coesite is the green-yellow and commonly forms granular textures. E) Granular coesite, which contains dark, amorphous carbon centers (blue arrow). F) Granular coesite within  $\text{SiO}_2$  glass. Position of this image is marked by the box in (D).

### Thin-Section Petrography

In thin section, these two phases can be identified as silica glass and coesite. The silica glass is isotropic in cross-polarized light and in plane-polarized light lacks the flow textures. Texturally, the coesite aggregates have

two general morphologies (1) isolated individual aggregates embedded within the glass (Figs. 2D–F), and (2) a closely packed network of aggregates (Figs. 2B and 2C). This coesite network commonly forms on the edges of the vesicle, but occasionally occurs in the center of an amygdule (Figs. 2B and 2D). Coesite

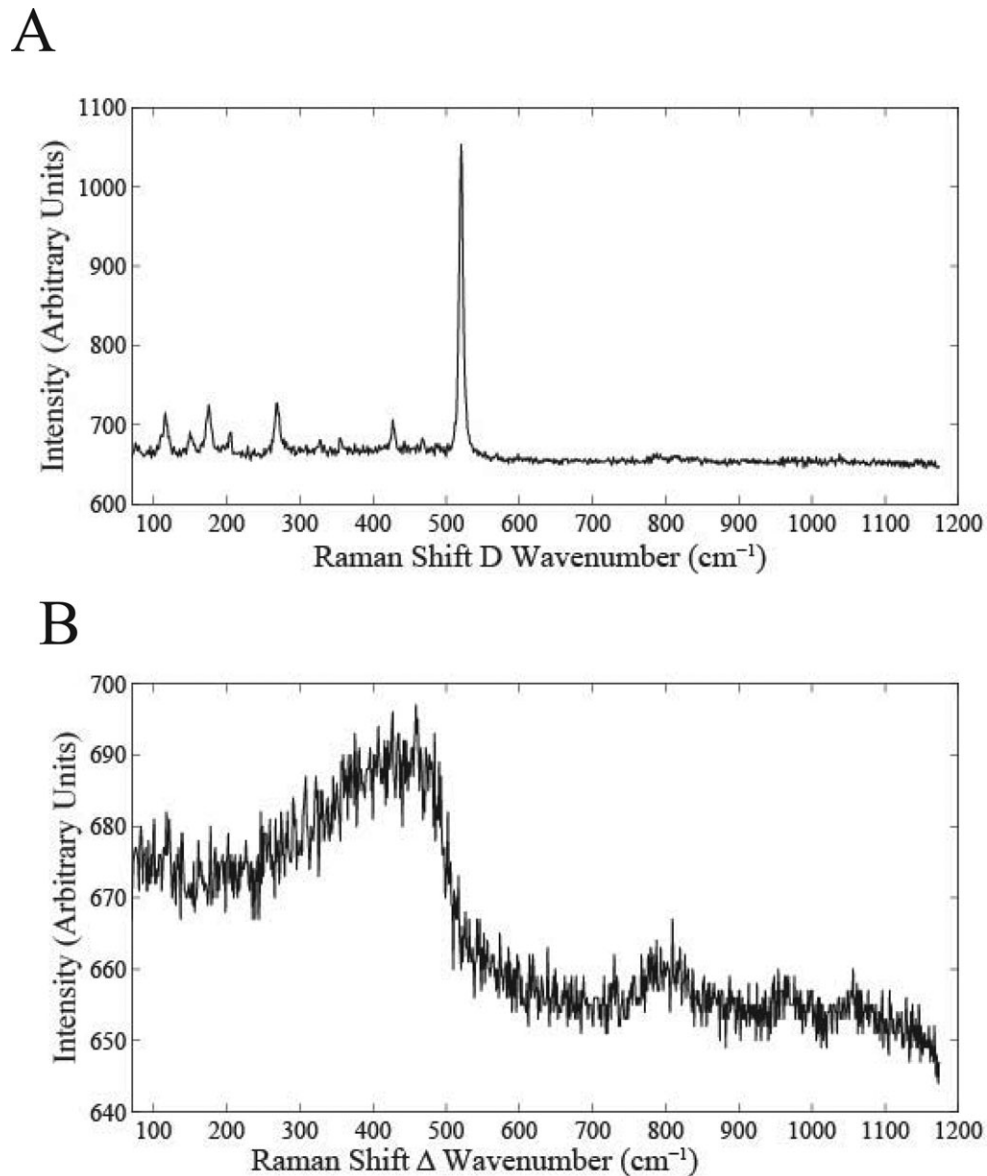


Fig. 3. Raman spectra of (A) coesite and (B)  $\text{SiO}_2$  glass.

occurs as 30–40  $\mu\text{m}$  high-relief, greenish-brown spherical aggregates of smaller crystallites (Figs. 2E and 2F). In some instances, coesite aggregates appear to be nucleating around smaller crystallites. Additionally, some granular coesite aggregates have opaque grains (identified below as amorphous carbon) in the center of the sphere (Fig. 2E).

### Raman Spectroscopy

Micro-Raman spectroscopy was used to identify phases within the silica vugs: crystalline coesite, an  $\text{SiO}_2$  glass, and a rare amorphous carbon phase. The

crystalline coesite is characterized by vibrational modes showing peaks at 113, 173, 267, and 429  $\Delta\text{cm}^{-1}$ , and a strong Si-O mode at  $\Delta 521 \text{ cm}^{-1}$  (Fig. 3). The  $\text{SiO}_2$  glass is characterized by a broad peak near 449  $\Delta\text{cm}^{-1}$ , and a substantial drop-off in intensity at 494  $\Delta\text{cm}^{-1}$  (Fig. 3). Micro-Raman imaging with high spatial resolution indicates that the aggregates of granular coesite are in fact microcrystallites. Spectra acquired with spot size of 763 nm show both the broad peak near 449  $\Delta\text{cm}^{-1}$  and a strong peak at 521  $\Delta\text{cm}^{-1}$ , which is consistent with a mix of coesite plus amorphous  $\text{SiO}_2$  (Fig. 4). In some instances, granular coesite contains opaque grains in the center, which display micro-Raman spectra indicative of

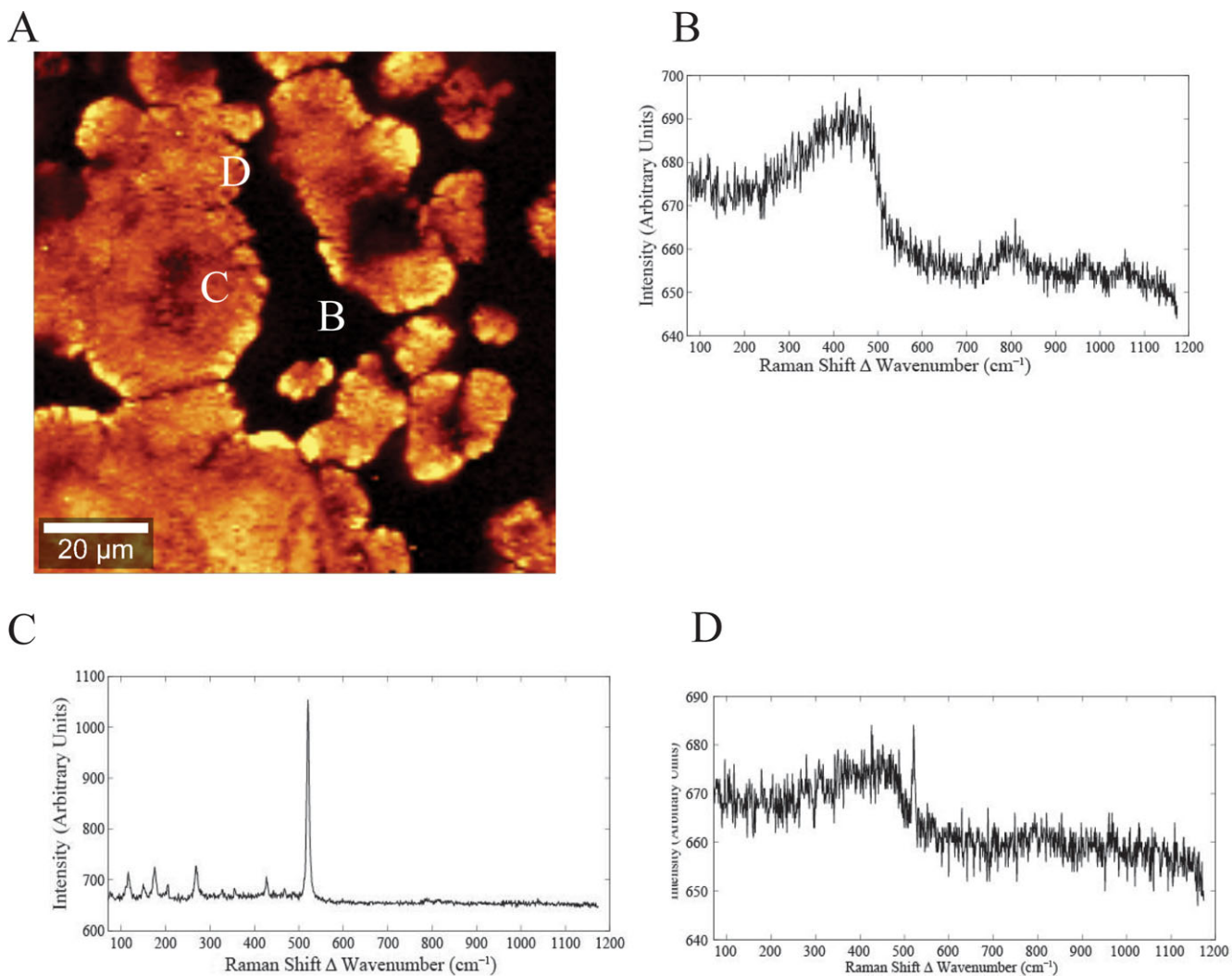


Fig. 4. Raman map (A) and spectra of SiO<sub>2</sub> glass (B), coesite (C), and a mix of coesite+glass (D). Locations of spectra are indicated by associated letters.

a carbon phase (i.e., amorphous carbon D and G bands with peaks at 1360 and 1560 cm<sup>-1</sup> (Fig. 5) (Ferrari 2007).

### NMR Spectroscopy

NMR spectroscopy indicates that the vug silica occurs in several distinct environments that likely include crystalline and two amorphous phases. The spectra (Fig. 6A) contain a main peak centered near -112 ppm; a broad shoulder near -105 ppm; and small, narrow peaks at -108.5 and -114.3 ppm. The <sup>29</sup>Si chemical shift of the second broad peak, -105 ppm, is consistent with a diaplectic silica-rich glass. Based on the NMR results, we estimate that the vug filling consists of 26% coesite, 52% fused silica, and 22% of the second amorphous phase, a densified diaplectic silica glass (see Discussion section).

### DISCUSSION

Importantly, interpretation of the SiO<sub>2</sub> phases in the vugs requires multiple techniques.

Optical petrography and micro-Raman spectroscopy indicate two Si-phases: coesite+SiO<sub>2</sub> glass. NMR spectroscopy, however, indicates three phases: coesite plus two different silica-rich glass phases. Although the two SiO<sub>2</sub> glass phases cannot be distinguished from each other petrographically, they can be distinguished with NMR based on different local chemical environments indicative of different formation mechanisms.

### NMR Spectroscopy

The <sup>29</sup>Si NMR chemical shifts of the two narrow peaks and their occurrence in near-equal intensity is

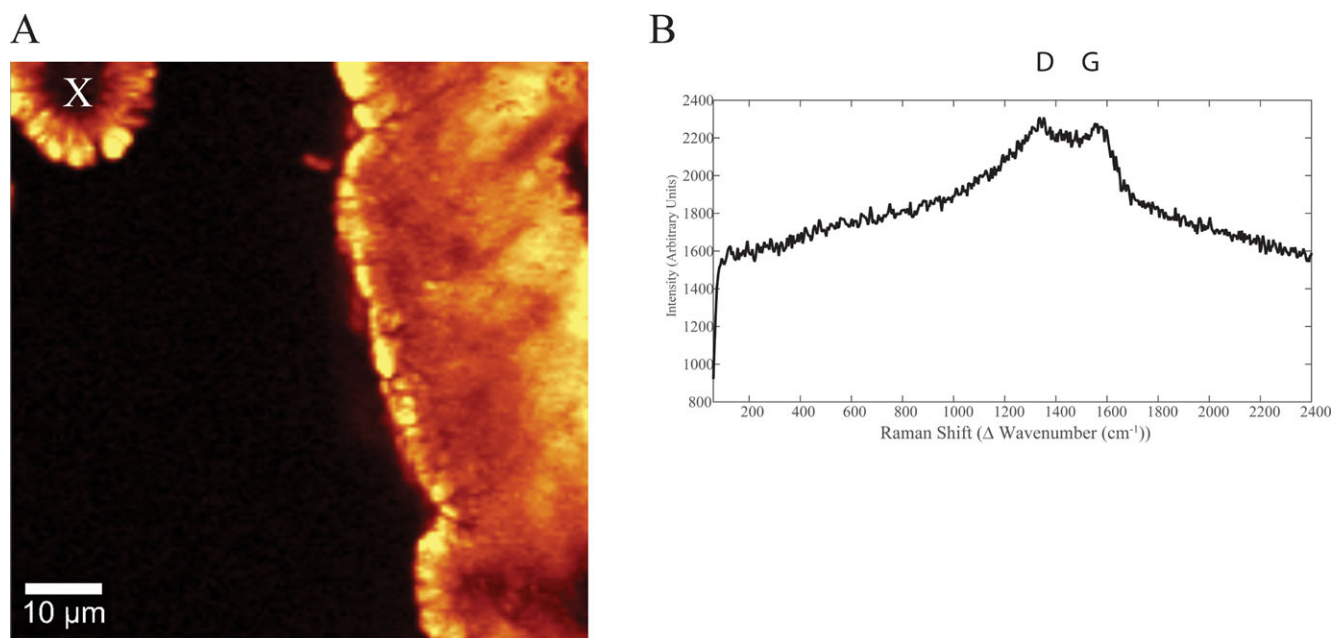


Fig. 5. Raman map (A) and spectra of coesite with dark opaque centers (B). The centers are amorphous carbon, as indicated by the D and G Raman bands.

consistent with previous results reported for crystalline coesite (Smith and Blackwell 1983), and for coesite present in the Coconino sandstone impactite at Meteor Crater (Yang et al. 1986). A spectrum taken with a 1000 s relaxation delay (data not shown) is essentially identical except for somewhat higher intensity of the narrow peaks. A least-squares fit of the spectrum taken at 100 s relaxation delay (Figs. 6B and 6C) yielded peak positions for the two broad peaks of  $-105$  and  $-112$  ppm and widths of 12.6 and 9.3 ppm FWHM, respectively. These large peak widths indicate the signals arise from amorphous substances.

Based on previous work we can propose assignment of the main peak at  $-112$  ppm to amorphous silica. Numerous previous  $^{29}\text{Si}$  NMR studies of fused silica yield a small range of chemical shifts near  $-112$  ppm (e.g., Oestrike et al. 1987; Mahler and Sebald 1995), but with widths generally closer to 12 ppm FWHM (see Malfait et al. [2008] for a summary). For a commercial  $\text{SiO}_2$  glass, Mahler and Sebald (1995) report a chemical shift of  $-111.8$  ppm and width 9.5 ppm FWHM, values similar to those we observe for the most intense broad peak. In contrast, for quartz recovered from shock experiments up to 38 GPa Fiske et al. (1998) report chemical shifts higher (less negative) than  $-110$  ppm. The width of the peak from deformed quartz increases with increasing shock pressure (Fiske et al. 1998) but is smaller than for the peak at  $-112$  for the present sample. These comparisons indicate that the spectral characteristics of the main peak at  $-112$  ppm more

closely resemble those of fused silica than shock-deformed quartz.

The  $^{29}\text{Si}$  chemical shift of the second broad peak,  $-105$  ppm, is consistent with either diaplectic silica-rich glass or an alkali aluminosilicate glass. For quartz recovered from shock experiments at pressures above 30 GPa, Fiske et al. (1998) observe a second peak at higher chemical shifts that was assigned to diaplectic glass, in addition to the signal from deformed quartz. For example, quartz subjected to 33 GPa shock loading yielded  $^{29}\text{Si}$  NMR peaks at  $-109.9$  ppm for deformed quartz and a broad shoulder at  $-107.8$  ppm for diaplectic glass. For  $^{29}\text{Si}$  NMR, higher (less negative) chemical shifts correspond to smaller average Si–O–Si bond angles, consistent with denser material. Fiske et al. (1998) also report that a fused silica sample that had been statically compressed to 18 GPa at ambient temperature yields a  $^{29}\text{Si}$  chemical shift of  $-105.6$  ppm, consistent with the idea that densified silica-rich glass is characterized by higher  $^{29}\text{Si}$  NMR chemical shifts. Framework alkali aluminosilicate glasses can also yield  $^{29}\text{Si}$  NMR chemical shifts similar to that of the smaller broad peak (Oestrike et al. 1987), for example,  $-104.9$  ppm for glass of approximately equimolar albite-orthoclase-silica composition. In this case the higher chemical shift compared to fused silica results from Al substitution in the tetrahedra adjacent to and corner-shared with the silicate tetrahedron. This overlap of chemical shift ranges for different materials prevents the nature of the second amorphous phase from being

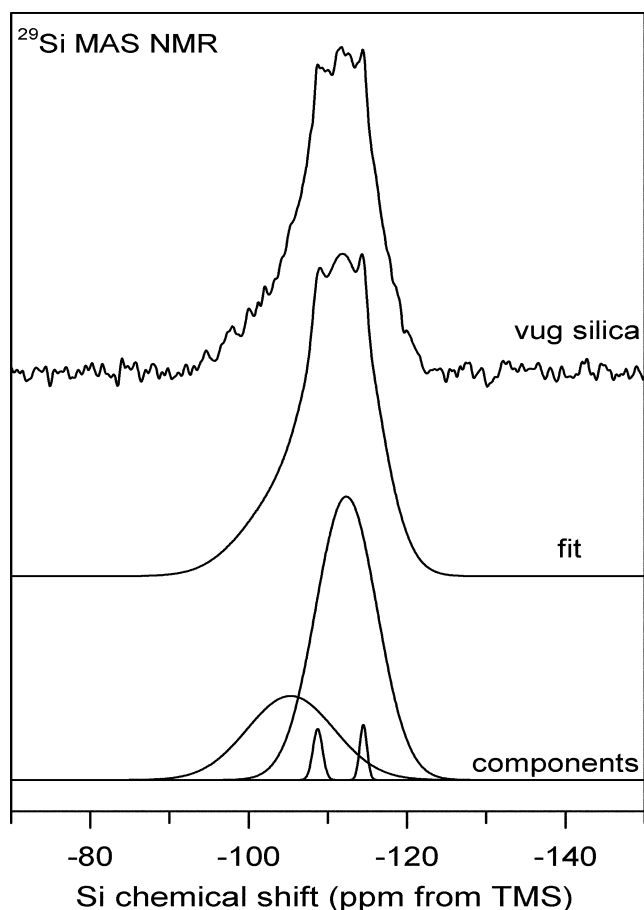


Fig. 6.  $^{29}\text{Si}$  MAS/NMR spectrum of silica-rich amygdule, showing the presence of peaks for coesite (narrow peaks) and two amorphous phases (broad peak near  $-112$  ppm and broad shoulder near  $-105$  ppm). A) Observed spectrum acquired at a spinning rate of 12 kHz and a 100 s relaxation delay for a total of 4176 acquisitions. B) least-squares fit of the spectrum in (A) composed of four Gaussian peaks (C).

determined solely from its  $^{29}\text{Si}$  NMR chemical shift. However, absence of a significant  $^{27}\text{Al}$  MAS/NMR signal from the sample indicates that Al is not a major component, thereby allowing us to rule out the possibility of this being an aluminosilicate glass.

Estimation of the relative proportions of the three detected phases is complicated by clear evidence for differential relaxation effects between the crystalline coesite and the amorphous phases. The coesite peaks represent  $3 \pm 1\%$  of the integrated intensity in the spectrum taken with a 100 s relaxation delay and  $5 \pm 1\%$  for that at 1000 s. This relative increase is similar to, but somewhat smaller than the factor of two increase observed by Myers et al. (1998) for coesite in an NMR relaxation study of the Coconino sandstone. That study found that complete relaxation of the coesite  $^{29}\text{Si}$  NMR signal required  $\sim 20,000$  s, and that at 1000 s the signal had recovered to 22% of its equilibrium value.

Assuming the present sample exhibits similar relaxation properties and that the amorphous phases are fully relaxed at 1000 s, we estimate that  $\sim 26\%$  of the Si occurs in coesite. The smaller differential relaxation we observed from 100 to 1000 s compared to Myers et al. (1998) suggests that the relaxation rate is faster for the present sample, in which case this estimate represents a maximum value for the abundance of coesite. Relaxation rates are highly dependent on the impurity concentration, so accurate proportions require acquisition of fully relaxed spectra that is impractical for the presently available amount of sample. The ratio of integrated intensity of the two broad peaks does not change appreciably from 100 to 1000 s of relaxation, giving values of 2.39 and 2.35. This similarity suggests that both signals are nearly fully relaxed at 100 s, because it is unlikely for separate phases to yield nearly identical relaxation rates. Given these estimates and caveats, we estimate that the vug filling consists of 26 mole% coesite, 52 mole% fused silica, and 22 mole% of the second amorphous phase, interpreted to be a densified diaplectic silica glass.

#### Texture and Formation Conditions

The coesite at Lonar exhibits an unusual texture: concentration of granular coesite along preimpact vesicle walls (as an apparent rind) and in densely packed regions near or at the center of the  $\text{SiO}_2$  glass. There are multiple possible explanations for this texture (1) concentration of stress (or P, and T) at the edges and center of the vug due to interactions between the shock wave and the vesicle wall/vug, (2) nucleation of coesite against the vesicle wall, and/or (3) impurities or heterogeneities within the glass serving as a nucleation point for coesite. The extreme heterogeneity among vugs in these samples suggests it is likely that all three possibilities are contributing to the texture of the coesite at Lonar. Shock waves are known to refract when passing through geologically complex materials and there is likely a great contrast between the basalt and vug (particularly if the filling is opalline silica). Generally speaking, nucleation fronts are also common—particularly along surfaces that serve as energy minima for initiation of crystallization. Last, in these samples, we see an uneven distribution of carbon phases (Fig. 7), which suggest there is a heterogeneous distribution of impurities, and these impurities are frequently the site of nucleation of the coesite (Fig. 2E).

Our work highlights the importance of technique when interpreting glass components within impact samples. In impact settings, glass can be produced in two ways—as a solid-state transformation (i.e., diaplectic glass) or as a fused glass. The formation conditions of these glass types are different and there

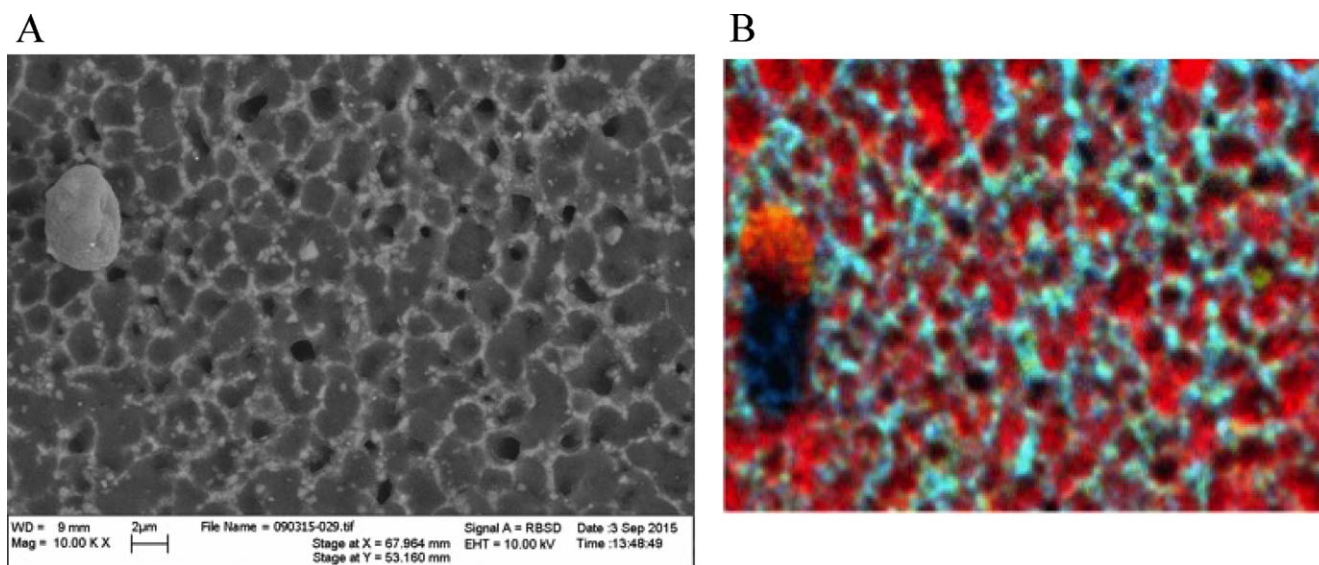


Fig. 7. SEM image (A) and map (B) of carbon-rich  $\text{SiO}_2$  glass and coesite.

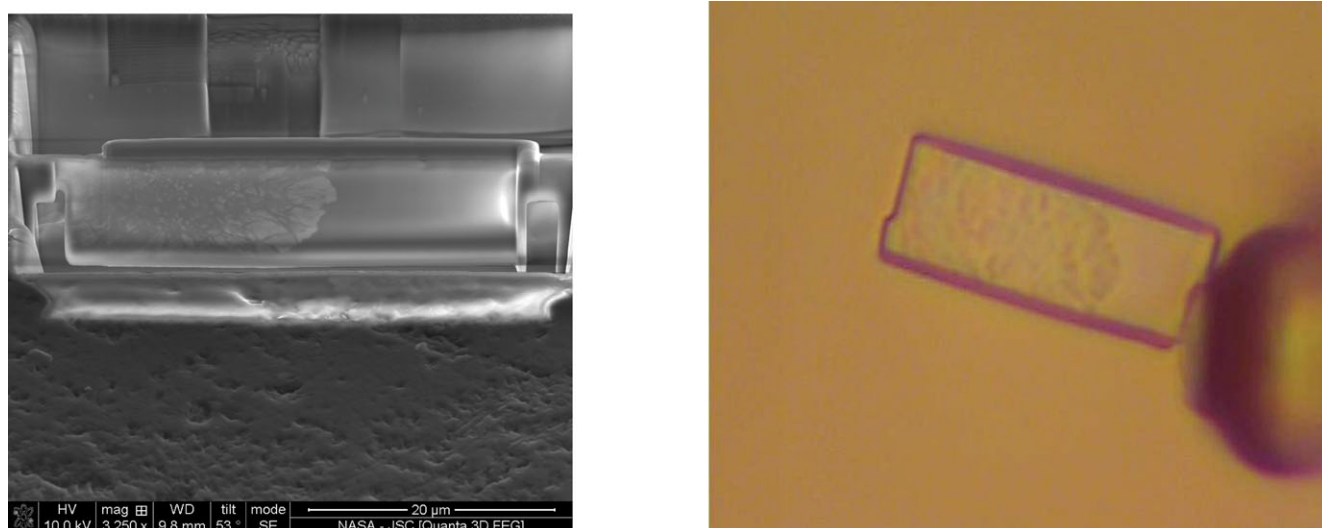


Fig. 8. Focused Ion Beam slices of coesite+glass. A) Secondary ion image of polished slab. B) Transmitted light image of the FIB foil mounted on a needle. In both instances the granular texture of the coesite is visible.

are important geochemical and structural differences between fused glass and a glass formed by solid-state processes. As shown by our data, relying on optical petrography or Raman spectroscopy alone may not be sufficient to interpret exact formation conditions.

Coesite at Lonar is found only within former amygdules of the basalts, suggesting the  $\text{SiO}_2$  precursor phase was a preshock secondary phase. Preimpact alteration and precipitation of secondary minerals including zeolite, quartz, opaline silica, chalcedony, and tridymite is common in the target Deccan basalts at Lonar (Sukheswala et al. 1974). The presence of coesite

here represents the first direct observation of a terrestrial shocked secondary mineral. Secondary silica was suggested as the source for coesite within melt-breccias at the Vredefort impact structure (Martini 1991), but direct petrographic evidence is lacking.

The presence of coesite in impact materials is often used as an indicator of impact conditions, specifically pressures and temperatures (e.g., French 1998). However, in these specific samples, shock barometry may be complicated by a series of factors. First, common secondary minerals in the Deccan basalts at Lonar include both opaline silica and quartz. Because all the

SiO<sub>2</sub> present in these samples has been transformed to coesite+glass, it is not possible to determine the starting preshock SiO<sub>2</sub> phase. The specific starting phase likely affects exact formation conditions. For example, it is common for experimental studies of coesite to start with amorphous SiO<sub>2</sub> because synthesizing coesite from an amorphous material rather than quartz is energetically more favorable. Similarly, addition of Si-OH changes formation conditions of coesite (Zhang et al. 2008), and water content is known to change the conditions under which coesite can form in impact settings (Osinski 2007).

Even if we assume that the coesite forms as a replacement after quartz, the specific P-T conditions remain unclear. Currently, there is debate as to how coesite forms in impact settings—as either a solid-state transformation (Stöffler 1971; Ferrière and Osinski 2013) or as the crystallization from a melt (Chen et al. 2010). The texture of the coesite in these Lonar basalt samples, particularly the isolated granular coesite within the glass, is consistent with textures at the Xiuyan impact structure, which Chen et al. (2010) interpret as having crystallized from a melt. Also consistent with this is the microcrystallites, which appear to be nucleating (in some instances against a carbon phase; Figs. 2E and 5). Secondary electron images in the FIB show granular coesite is an aggregate of submicron grains embedded within the glass. Textures of the nanocrystallites suggest nucleation from a rapidly quenched melt (Fig. 8).

Furthermore, our NMR data suggest at least one of the glass phases is a fused silica glass, so interpreting the coesite as crystallizing from a melt is not unreasonable because our NMR results would seem to require that at least one of the two SiO<sub>2</sub> glasses is a melt product. This is based on the lack of compositional difference between the two detected amorphous phases.

Impact melt, however, is not consistent with the bulk texture of this sample. This sample is classified as shock Class 2 (Kieffer et al. 1976; Wright et al. 2011; Jaret et al. 2015), defined by the presence of maskelynite, which lacks flow texture. Importantly, preservation of zoning in the maskelynite and the presence of remnant anisotropy in the maskelynite indicates that the plagioclase was transformed to glass via solid-state transformations (Jaret et al. 2015).

We can reconcile this discrepancy between the SiO<sub>2</sub> phases suggesting formation from a melt and bulk-rock textures of the solid-state maskelynite by considering the petrographic context of the SiO<sub>2</sub> phases. In these samples, coesite occurs only within preimpact amygdules, and thus we interpret these as areas of extremely localized melting associated with the vesicle.

Analysis of experimentally and naturally shocked porous sandstones has shown that during shock,

collapsing pore space can cause localized increases in pressure and temperature and can trigger local melting, as suggested for the Coconino Sandstone at Meteor Crater (Kieffer 1971). Similarly, at Vredefort, coesite is associated with melt within pseudotachylite, and interpreted to have formed due to local heating associated with collapsing fractures during shock. Grain-boundary interactions between the shock wave, individual grains, and pore space cause localized concentrations of stress (and pressure and temperature) at grain margins, such that shock events in porous rocks deposit more energy than in nonporous materials. The samples from Lonar studied here are not exactly like porous sandstones, but a similar process may occur due to collapsing space within and adjacent to the vesicle.

The association of melt with high-pressure polymorphs in impact settings may be more widespread than previously recognized. Interestingly, at Bosumtwi, some coesite inclusions in diaplectic SiO<sub>2</sub> glass occur in grains that are directly adjacent to melt (Morrow 2007), and the coesite formation may indeed be tied to heating from adjacent melt. A similar phenomenon occurs with high-pressure feldspar phases in meteorites where those high-pressure phases occur in association with melt veins and pockets, as has been suggested for the formation of tissintite (Walton et al. 2014).

At Lonar, the local melting is not associated with fractures, but instead vugs, which may provide a new opportunity to look for high-pressure phases. If collapsing vesicles or concentration of stress as the shock wave interacts with the vesicles and fillings generate heat during shock, as suggested here, then one might expect to find similar evidence of melt or high-pressure phases in shocked vesicular meteorites or terrestrial impacts into vesicular targets.

## CONCLUSIONS

Here we present the first observation of coesite at the Lonar crater and address its significance. Coesite is confined to within former silica amygdules in the target vesicular basalts. This work is also the first report of high-pressure phases found in a shocked secondary precipitate. The coesite occurs as 30–40 μm aggregates of smaller crystallites, interpreted as having crystallized directly from a melt. <sup>29</sup>Si NMR results suggest the coesite occurs in association with two distinct silica-rich glass phases, one of which is a quenched melt (at low P). Impact melting, however, is inconsistent with the bulk-rock textures, which show no large-scale flow textures and these samples contain maskelynite grains, which preserve original igneous zoning, and infrared anisotropy. We reconcile these discrepancies by the petrographic context of the coesite and silica fused

glass, which are confined only to the vesicles. Therefore, we suggest extremely localized melting, caused by collapsing vesicles during shock.

*Acknowledgments*—The FIB work was completed in the Electron Beam Analysis Labs within the Astromaterials Research and Exploration Science Office at the NASA Johnson Space Center. This manuscript benefited from discussion with Hanna Nekvasil (Stony Brook University), and the Stony Brook University Planetary Geology discussion group. We also thank J. W. Horton and A. El Goresy for insightful reviews. This work was supported by the RIS<sup>4</sup>E team of the Solar System Exploration Research Virtual Institute (PI T. Glotch). This is SSERVI Publication number SSERVI-2016-062. All data in this paper will be archived and made available on the Stony Brook University Vibrational Spectroscopy Laboratory's website: <http://aram.ess.sunysb.edu/tglotch>.

*Editorial Handling*—Dr. Christian Koeberl

## REFERENCES

- Bandfield J. L., Hamilton V. E., and Christensen P. R. 2000. A global view of Martian surface compositions from MGS-TES. *Science* 287:1626–1630.
- Bohor B. F., Betterton W. J., and Foord E. E. 1988. Coesite, glass, and shocked quartz at DSDP Site 612: Evidence for nearby impact in the Late Eocene. Proceedings, 26th Lunar and Planetary Science Conference. p. 114.
- Boslough M. B., Cygan R. T., and Kirkpatrick R. J. 1993. <sup>29</sup>Si NMR spectroscopy of naturally shocked quartz from Meteor Crater, Arizona: Correlation to Kieffer's classification scheme. Proceedings, 24th Lunar and Planetary Science Conference. pp. 149–150.
- Boslough M. B., Cygan R. T., and Izett G. A. 1995. NMR spectroscopy of shocked quartz from the K/T boundary: Shock-induced peak broadening, dense glass, and coesite. Proceedings, 26th Lunar and Planetary Science Conference. pp. 149–150.
- Boyer H., Smith D. C., Chopin C., and Lasnier B. 1985. Raman microprobe (RMP) determinations of natural and synthetic coesite. *Physics and Chemistry of Minerals* 12:45–48.
- Bunch T. E. and Cohen A. J. 1963. Coesite and shocked quartz from Holleford Crater, Ontario, Canada. *Science, New Series* 142:379–381.
- Chao E. C. T., Shoemaker E. M., and Madsen B. M. 1960. First natural occurrence of coesite. *Science* 132:220–222.
- Chao E. T. C., Fahey J. J., and Littler J. 1961. Coesite from Wabar Crater, near Al Hadida, Arabia. *Science* 133:882–883.
- Chao E. T. C., Fahey J. J., Littler J., and Milton D. J. 1962. Stishovite, SiO<sub>2</sub>, a very high pressure new mineral from Meteor Crater, Arizona. *Journal of Geophysical Research* 67:419–421.
- Chen M., Xiao W., and Xie X. 2010. Coesite and quartz characteristics of crystallization from shock produced silica melt in the Xiuyan Crater. *Earth and Planetary Science Letters* 297:306–314.
- Chopin C. 1984. Coesite and pure pyrope in high-grade blueschists of the Western Alps: A first record and some occurrences. *Contributions to Mineralogy and Petrology* 86:107–118.
- Coes L. Jr. 1953. A new dense crystalline silica. *Science* 118:131–132.
- Cohen A. J., Bunch T. E., and Reid A. M. 1961. Coesite discoveries establish cryptovolcanics as fossil meteorite craters. *Science* 134:1624–1625.
- Cygan R. T., Boslough M. B., and Kirkpatrick R. J. 1990. NMR spectroscopy of experimentally shocked quartz: shock wave barometry. Proceedings, 20th Lunar and Planetary Science Conference. pp. 451–457.
- Cygan R. T., Boslough M. B., and Kirkpatrick B. J. 1992. NMR spectroscopy of experimentally shocked quartz and feldspar powders. Proceedings, 22nd Lunar and Planetary Science Conference. pp. 127–136.
- Dachille F., Zeto R. J., and Roy R. 1963. Coesite and stishovite: Stepwise reversal transformations. *Science* 140:991–993.
- De Carli P. S. and Milton D. J. 1965. Stishovite, synthesis by shock wave. *Science* 165:144.
- Dence M. R., Robertson P. B., and Wirthlin R. L. 1974. Coesite from the Lake Wanapitei crater, Ontario. *Earth and Planetary Science Letters* 22:118–122.
- El Goresy A., Gillet P., Chen M., Stahle V., and Graup G. 2001a. In situ finding of the loci of the fabric settings of shock induced quartz/coesite phase transformation in crystalline clasts in Suevites of the Ries Crater, Germany. 64th Annual Meteoritical Society Meeting, Abstract No. 5065.
- El Goresy A., Dubrovinsky L., Gillet P., and Chen M. 2001b. Natural post-rutile and post-stishovite polymorphs in shocked terrestrial and Martian rocks: Mode of occurrence, structural analogies and formational mechanisms. American Geophysical Union, Fall Meeting 2001, abstract #T22E-10.
- El Goresy A., Dera P., Sharp T. G., Prewitt C. T., Chen M., Dubrovinsky L., Wopenka B., Boctor N. Z., and Hemley R. J. 2008. Seifertite, a dense orthorhombic polymorph of silica from the Martian meteorites Shergotty and Zagami. *European Journal of Mineralogy* 20:523–528.
- Engelhardt W. von and Stöffler D. 1968. Stages of shock metamorphism in crystalline rocks of the Ries Basin, Germany. In *Shock metamorphism of natural materials*, edited by French B. M. and Short N. M. Baltimore, Maryland: Mono Book Corp. pp. 159–168.
- Fazio A., Folco L., D'Orazio M., Frezzotti M. L., and Cordier C. 2014. Shock metamorphism and impact melting in small impact craters on Earth: Evidence from Kamil crater, Egypt. *Meteoritics & Planetary Science* 49:2175–2200.
- Fei Y. and Bertka C. M. 1999. Phase transitions in the Earth's mantle and mantle mineralogy. In *Mantle petrology: Field observations and high pressure experimentation: A tribute to Francis R. (Joe) Boyd*, edited by Fei Y., Bertka C. M., and Mysen B. O. Houston, Texas: The Geochemical Society. pp. 189–207.
- Ferrari A. C. 2007. Raman spectroscopy of graphene and graphite: Disorder, electron-phonon coupling, doping and nonadiabatic effects. *Solid State Communications* 143:47–57.
- Ferrière L. and Osinski G. R. 2013. Shock metamorphism. In *Impact cratering: Processes and products*, edited by Osinski G. R. and Pierazzo E. Oxford: Wiley-Blackwell. 316 p.

- Ferrière L., Koeberl C., and Reimold W. U. 2009. Characterization of ballen quartz and cristobalite in impact breccias: New observations and constraints on ballen formation. *European Journal of Mineralogy* 21:203–217. doi:10.1127/0935-1221/2009/0021-1898.
- Fiske P. S., Nellis W. J., Xu Z., and Stebbins J. F. 1998. Shocked quartz: A  $^{29}\text{Si}$  magic-angle-spinning nuclear magnetic resonance study. *American Mineralogist* 83:1285–1292.
- Fredriksson K., Dube A., Milton D. J., and Balasundaram M. S. 1973. Lonar Lake, India: An impact crater in basalt. *Science* 180:862–864.
- French B. M. 1998. Traces of catastrophe: A handbook of shock-metamorphic effects in terrestrial meteorite impact craters. LPI Contribution 954. Houston, Texas: Lunar and Planetary Institute. 120 p.
- French B. M. and Koeberl C. 2010. The convincing identification of terrestrial meteorite impact structures: What works, what doesn't, and why. *Earth-Science Reviews* 98:123–170. doi:10.1016/j.earscirev.2009.10.009.
- Glass B. P. and Wu J. 1993. Coesite and shocked quartz discovered in the Australasian and North American microtektite layers. *Geology* 21:435–438.
- Gurov E. P. and Koeberl C. 2004. Shocked rocks and impact glasses from the El'gygytgyn impact structure, Russia. *Meteoritics & Planetary Science* 39:1495–1508.
- Gurov Y. P., Val'ter A. A., and Rakitskaya R. B. 1980. Coesite in rocks of meteorite explosion craters on the Ukrainian shield. *International Geology Review* 22:329–332.
- Gurov E. P., Gurova E. P., and Sokur T. M. 2002. Geology and petrography of the Zapandaya impact crater in the Ukrainian Shield. In *Impacts in Precambrian shields.*, edited by Pesonen L. J., and Plado J. New York: Springer.
- Heaney P. J., Prewitt C. T., and Gibbs G. V. (eds). 1994. Silica: Physical behavior, geochemistry, and materials applications. Reviews in Mineralogy, vol. 29. Washington, D.C.: Mineralogical Society of America. pp. 606.
- Hecht L., Reimold U. W., Sherlock S., Tagle R., Koeberl C., and Schmitt R.-T. 2008. New impact-melt rock from the Roter Kamm impact structure, Namibia: Further constraints on impact age, melt rock chemistry, and projectile composition. *Meteoritics & Planetary Science* 43:1201–1218.
- Horton J. W. Jr., Kunk M. J., Belkin H. E., Aleinikoff J. N., and Chou I.-M. 2009. Evolution of crystalline target rocks and impactites in the Chesapeake Bay impact structure, ICDP-USGS Eyrville B core. In *The ICDP-USGS Deep Drilling Project in the Chesapeake Bay impact structure: Results from the Eyreville Core Holes*, edited by Gohn G. S., Koeberl C., Miller K. G., and Reimold W. U. *GSA Special Paper* 458:277–316.
- Jackson J. C., Horton J. W., Chou I.-M., and Belkin H. E. 2016. Coesite in suevites from the Chesapeake Bay impact structure. *Meteoritics & Planetary Science* 51:946–965.
- Jaret S. J., Woerner W. R., Phillips B. L., Ehm L., Nekvasil H., Wright S. P., and Glotch T. D. 2015. Maskelynite formation via solid-state transformation: Evidence of infrared and X-ray anisotropy. *Journal of Geophysical Research* 120:570–587. doi:10.1002/2014JE004764.
- Jourdan F., Moynier F., Koeberl C., and Eroglu S. 2011.  $^{40}\text{Ar}/^{39}\text{Ar}$  age of the Lonar crater and consequences for the geochronology of planetary impacts. *Geology* 39:671–674.
- Kieffer S. W. 1971. Shock metamorphism of the Coconino sandstone at Meteor Crater, Arizona. *Journal of Geophysical Research* 76:5449–5473.
- Kieffer S. W., Schaal R. B., Gibbons R., Hörz F., Milton D. J., and Dube A. 1976. Shocked basalt from Lonar Impact crater, India, and experimental analogues. Proceedings, 7th Lunar and Planetary Science Conference. pp. 1391–1412.
- Kleeman J. D. and Ahrens T. J. 1973. Shock-induced transition of quartz to stishovite. *Journal of Geophysical Research* 78:5954–5960.
- Lakshatanov D. L., Sinogeikin S. V., Litasov K. D., Prakapenka V. B., Hellwig H., Wang J., Sanches-Valle C., Perrillat J.-G., Chen B., Somayazulu M., Li J., Ohtani E., and Bass J. D. 2007. The post-stishovite phase transition in hydrous alumina-bearing  $\text{SiO}_2$  in the lower mantle of the earth. *Proceedings of the National Academy of Sciences* 104:13,588–13,590.
- Lee S. K., Park S. Y., Kim H. I., Tschauer O., Asimow P., Bai L., Xiao Y., and Chow P. 2012. Structure of shock compressed model basaltic glass: Insights from O K-edge X-ray Raman scattering and high resolution  $^{27}\text{Al}$  NMR spectroscopy. *Journal of Geophysical Research* 39:L05306. doi:10.1029/2012GL050861.
- Lehtinen M. 1976. Lake Lappajärvi, a meteorite impact site in Western Finland. *Geological Survey of Finland Bulletin* 282:1–92.
- Levien L. and Prewitt C. T. 1981. High pressure crystal structure and compressibility of coesite. *American Mineralogist* 66:324–333.
- Littler J. 1962. *Coesite from the Lake Bosumtwi Crater, Ashanti*. Ghana: Geological Society of America Abstract.
- Liu L. and Bassett W. A. 1986. *Elements. Oxides and silicates*. New York: Oxford University Press.
- Lounejeva E., Ostroumov M., and Sánchez-Rubio G. 2002. Micro-Raman and optical identification of coesite in suevite from Chicxulub. *Geological Society of America Special Paper* 356:47–54.
- Lu Z., Zhang L., Du J., and Bucher K. 2008. Coesite inclusions in garnet from eclogitic rocks in Western Tianshan, Northwest China: Convincing proof of UHP metamorphism. *American Mineralogist* 93:1845–1850.
- Mahler J. and Sebald A. 1995. Deconvolution of  $^{29}\text{Si}$  magic-angle spinning nuclear magnetic resonance spectra of silicate glasses revisited—Some critical comments. *Solid State Nuclear Magnetic Resonance* 5:63–78.
- Malfait W. J., Halter W. E., and Verel R. 2008.  $^{29}\text{Si}$  NMR spectroscopy of silica glass: T1 relaxation and constraints on the Si-O-Si bond angle distribution. *Chemical Geology* 256:269–277.
- Maloof A. C., Stewart S. T., Weiss B. P., Soule S. A., Swanson-Hysell N. L., Louzada K. L., Garrick-Bethell L., and Poussart P. M. 2010. Geology of Lonar crater, India. *Geological Society of America Bulletin* 122:109–126.
- Martini J. E. J. 1978. Coesite and stishovite from the Vredefort Dome, South Africa. *Nature* 272:715–717.
- Martini J. E. J. 1991. The nature, distribution, and genesis of coesite and stishovite associated with pseudotachylite of the Vredefort Dome, South Africa. *Earth and Planetary Science Letters* 103:285–300.
- Masaitis V. L. 1999. Impact structures of Northeastern Eurasia: The territories of Russia and adjacent countries. *Meteoritics & Planetary Science* 34:691–711.
- Masaytis V. L., Mashchak M. S., and Sokolova I. Y. 1980. High pressure silica phases in the Ternovka Astrobleme. *Doklady Akademii Nauk SSSR* 255:164–167.

- Miyahara M., Ohtani E., Yamaguchi A., Ozawa S., Sakai T., and Hiaro N. 2014. Discovery of coesite and stishovite in eucrite. *Proceedings of the National Academy of Sciences* 111:10,939–10,942.
- Morrow J. R. 2007. Shock-metamorphic petrography and microRaman spectroscopy of quartz in upper impactite interval, ICDP Drill Core LB-07A, Bosumtwi Impact Crater, Ghana. *Meteoritics & Planetary Science* 42:591–609.
- Myers S. A., Cygan R. T., Assink R. A., and Boslough M. B. 1998.  $^{29}\text{Si}$  MAS NMR relaxation study of shocked coconino sandstone from Meteor Crater, Arizona. *Physics and Chemistry of Minerals* 25:313–317.
- Oestrike R., Yang W. H., Kirkpatrick R. J., Hervig R. L., Navrotsky A., and Montez B. 1987. High-resolution  $^{23}\text{Na}$ ,  $^{27}\text{Al}$ , and  $^{29}\text{Si}$  NMR spectroscopy of framework aluminosilicate glasses. *Geochimica et Cosmochimica Acta* 51:2199–2209.
- Ohtani E., Ozawa S., Miyahara M., Ito Y., Mikouchi T., Kimura M., Arai T., Sato K., and Hiraga K. 2011. Coesite and stishovite in a shocked lunar meteorite, Asuka 881757, and impact events in the lunar surface. *Proceedings of the National Academy of Sciences* 108:463–466.
- Osinski G. R. 2007. Impact metamorphism of  $\text{CaCO}_3$ -bearing sandstones at the Haughton structure, Canada. *Meteoritics & Planetary Science* 42:1945–1960.
- Ostroumov M., Faulques E., and Lounejeva E. 2002. Raman spectroscopy of natural silica in Chicxulub impactite, Mexico. *Comptes Rendus Geoscience* 334:21–26.
- Perrillat J. P., Daniel I., Lardeaux J. M., and Cardon H. 2003. Kinetics of the coesite±quartz transition: Application to the exhumation of ultrahigh-pressure rocks. *Journal of Petrology* 44:773–788.
- Ramsdell L. S. 1955. The crystallography of “coesite.” *American Mineralogist* 40:975–982.
- Sharma S. K., Simons B., and Yoder H. S. Jr. 1983. Raman study of anorthite, calcium Tschermak’s pyroxene, and gehlenite in crystalline and glassy states. *American Mineralogist* 68:1113–1125.
- Shoemaker E. M. and Chao E. C. T. 1961. New evidence for the impact origin of the Ries Basin, Bavaria, Germany. *Journal of Geophysical Research* 66:3371–3378.
- Smith D. C. 1984. Coesite in clinopyroxene in the caledonides and its implication for geodynamics. *Nature* 310:641–644.
- Smith J. V. and Blackwell C. S. 1983. Nuclear magnetic resonance of silica polymorphs. *Nature* 303:223–225.
- Smyth J. R. and Hatton C. J. 1977. A coesite-sanidine grosspyrite from the Roberts Victor kimberlite. *Earth and Planetary Science Letters* 34:284–290.
- Smyth J. R., Smith J. V., Artioli G., and Kvick A. 1987. Crystal structure of coesite, a high-pressure form of SiO<sub>2</sub>, at 15 and 298 K from single-crystal neutron and X-ray diffraction data: Test of bonding models. *Journal of Physical Chemistry* 91:988–992.
- Stähle V., Altherr R., Koch M., and Nasdala L. 2008. Shock-induced growth and metastability of stishovite and coesite in lithic clasts from Suevite of the Ries impact crater (Germany). *Contributions to Mineralogy and Petrology* 155:457–472.
- Stebbins J. F. and Xue X. 2014. NMR spectroscopy of inorganic earth materials. *Reviews in Mineralogy and Geochemistry* 78:605–653. doi:10.2138/rmg.2014.78.15.
- Stishov S. M. and Papova S. V. 1961. A new dense modification of silica. *Geochemistry* 10:923–926. Translated from *Geokhimiya* 837–839.
- Stöffler D. 1971. Progressive metamorphism and classification of shocked and brecciated crystalline rocks at impact craters. *Journal of Geophysical Research* 76:5541–5551. doi:10.1029/JB076i023p05541.
- Sukheswala R. N., Avasia R. K., and Gangopadhyay M. 1974. Zeolites and associated secondary minerals in the Deccan traps of Western India. *Mineralogical Magazine* 39:658–671.
- Svensson N. B. and Wickman F. E. 1965. Coesite from Lake Mien, Southern Sweden. *Nature* 497:1202–1203.
- Vishnevskiy S. A., Maslov M. A., Pal’chik N. A., and Ponomarev G. Y. 1977. Coesite in the rocks of the Kara Structure. *Doklady Akademii Nauk SSSR* 232:154–157.
- Vishnevskiy S. A., Raitala J., Gibsher N. A., Ohman T., and Pal’chik N. A. 2006. Impact tuffites of the Popigai Astrobleme. *Russian Geology and Geophysics* 47:715–733.
- Walton E. L., Sharp T. G., Hu J., and Filiberto J. 2014. Heterogeneous mineral assemblages in Martian meteorite Tissint as a result of a recent small impact event on Mars. *Geochimica et Cosmochimica Acta* 140:334–348.
- Wright S. P. 2013. Decompression cracks in altered basalt under solid-state shock pressures: A new macroscopic shock texture (abstract #1010). 44th Lunar and Planetary Science Conference. CD-ROM.
- Wright S. P., Christensen P. R., and Sharp T. G. 2011. Laboratory thermal emission spectroscopy of shocked basalt from Lunar crater, and implications for Mars orbital and sample data. *Journal of Geophysical Research* 116:E09006. doi:10.1029/2010JE003785.
- Yang W. H., Kirkpatrick R. J., Vergo N., McHone J., Emilsson T. I., and Oldfield E. 1986. Detection of high-pressure silica polymorphs in whole-rock samples from a Meteor Crater, Arizona, impact sample using solid-state Si-29 nuclear magnetic resonance spectroscopy. *Meteoritics* 21:117–124.
- Zhang J., Li B., Utsumi W., and Liebermann R. C. 1996. In situ x-ray observations of the coesite-stishovite transition: Reversed phase boundary and kinetics. *Physics and Chemistry of Minerals* 23:1–10.
- Zhang G., Xu Y., Xu D., Wang D., Xue Y., and Su W. 2008. Pressure-induced crystallization of amorphous SiO<sub>2</sub> with silicon–hydroxy group and the quick synthesis of coesite under lower temperature. *High Pressure Research* 28:641–650.

## SUPPORTING INFORMATION

Additional supporting information may be found in the online version of this article:

**Figure S1.**  $^{29}\text{Si}$  MAS/NMR spectra of silica-rich vesicle filling taken at different relaxation delays as indicated. Spectra acquired with 4  $\mu\text{s}$  pulses ( $\pi/2$ ) at a 12 kHz spinning rate for a total of 414 (1000 s), 4176 (100 s), and 142,704 (s) acquisitions.